Author(s): Kauppinen, Toni; Laine, Petteri; Välikangas, Juho; Tynjälä, Pekka; Hu, Tao; Salminen, Justin; Lassi, Ulla

Title: Co-precipitation of NCM 811 Using Recycled and Purified Manganese : Effect of Impurities on the Battery Cell Performance

Year: 2023

Version: Published version

ChemElectroChem

Research Article
doi.org/10.1002/celc.202300265

Chemistry Europe
European Chemical Societies Publishing

www.chemelectrochem.org

Special Collection

Co-precipitation of NCM 811 Using Recycled and Purified Manganese: Effect of Impurities on the Battery Cell Performance

Toni Kauppinen,[a, b] Petteri Laine,[a] Juho Välikangas,[a] Pekka Tynjälä,[a, b] Tao Hu,[a] Justin Salminen,[c] and Ulla Lassi*[a, b]

Co-precipitation of NCM811 precursors and cathodes for lithium-ion batteries was carried out using recycled and purified manganese solution. In this paper, the aim is to study the role of the impurities in the co-precipitation step of NMC811 and further in the battery cell performance. Based on the results, cationic impurities (Ca, Zn, Mg, and Fe) are co-precipitated in the NMC811 precursors, as expected based on the thermodynamic considerations. The presence of these impurities was confirmed by several characterizations. Impurities did not affect the particle morphology or tap density of NMC811. Impurities had surprisingly minor effect on the cell performance. During the cycling, these cells provided good cyclability and high-capacity retention after 1100 cycles compared to reference samples.

Introduction

Since the mid-1990's, the amount of portable electronics, such as mobile phones, has increased. During mid-2000s number of smart phones started to increase greatly. Ever since smart phone era there has been constant demand for higher battery capacity. Alongside in the mid-2010s registration of electric vehicles started to increase.[1,2] In the early 1990s dominant cathode chemistry was $LiCoO_2$ with specific capacity of 140 mAhg/g.[3] Since then the trend has been to lower cobalt content of the cathode materials and increase the nickel content to achieve higher specific capacities and lower costs. Pure $LiNiO_2$ is attractive cathode material due to its high specific capacity (275 mAhg/g).[4,5] However, without any transition metal additives, $LiNiO_2$ seems to be unstable. Nickel tends to mix into lithium layer and vice versa (cation mixing), which makes it difficult to produce $LiNiO_2$ with stoichiometric Li:Ni ratio.[6] Secondly, when lithium content of the cathode material is low, it becomes unstable.[3] Nickel can be substituted with different transition metals. Cobalt and manganese have been the most popular in commercial cathode materials. Composition of commercial cathode materials have shifted from $LiCoO_2$, through $LiCo_{1/3}Ni_{1/3}Mn_{1/3}O_2$ and $LiNi_{0.6}Co_{0.2}Mn_{0.2}O_2$ to high-nickel $LiNi_{0.8}Co_{0.1}Mn_{0.1}O_2$.[7,8]

Cobalt substitution gives stabilizing effect on $LiNiO_2$ by decreasing likelihood for loss of oxygen in layered structure. Negative effect of the cobalt substitution is loss of conductivity. Although cobalt addition to $LiNiMnO_2$ unexpectedly increased conductivity of the material. Negative aspect of use of cobalt in Li-ion batteries, is its availability and relatively high cost. Abundant manganese is a key raw material for lithium-ion batteries, even though it is electrochemically inactive.[9] Mn stabilizes $LiNiO_2$ structure, allows cobalt to improve conductivity of the mixed cathode material, improves thermal stability at higher temperatures and is the most inexpensive of these three transition metal elements. However, replacing some of the nickel with manganese helps to keep costs low and similarly replacing a relatively small amount of the nickel with cobalt to stabilize the structure and to maintain capacity seem to be a good option.[9,10]

Role of impurities in the co-precipitation, and further in the battery cell performance is not much studied. Instead, there are several studies related to use of different metal dopants for battery performance. Weng et al.[7] investigated the influence of Mg to NCM cathode material. They synthesized $Li[Ni_{1/3}Co_{1/3}Mn_{1/3}]_{1-x}Mg_xO_2$ ($x = 0$, 0.01, 0.025, 0.05) cathode materials by adding $MgSO_4$ dopant during the co-precipitation process. Synthetized materials had all spherical particle shape. Study of electrochemical properties showed that the reversible capacities of the Mg doped cells decreased with the increasing Mg^{2+} content. Mg was found to improve the cycling performance at low content ($x \leq 0.01$) but high content of Mg ($x \geq 0.025$) led to capacity and cyclability loss because of uneven distribution of Mg^{2+} ions in the material. Weng et al.[7] concluded that if the concentration of Mg stays under 360 mg/L in the feed solution,

[a] T. Kauppinen, P. Laine, J. Välikangas, Dr. P. Tynjälä, Dr. T. Hu, Prof. U. Lassi
University of Oulu
Research unit of Sustainable chemistry
P.O.Box Oulu, 3000, 90014 (Finland)
E-mail: ulla.lassi@oulu.fi

[b] T. Kauppinen, Dr. P. Tynjälä, Prof. U. Lassi
University of Jyvaskyla
Kokkola University Consortium Chydenius
Talonpojankatu 2B, 67100 Kokkola (Finland)

[c] Dr. J. Salminen
Boliden Kokkola
Sinkkiaukio 1, 67100 Kokkola (Finland)

Special Collection An invited contribution to a Special Collection dedicated to NordBatt 2022 conference

the presence of Mg^{2+} in the final cathode materials stays under acceptable concentration ($x \leq 0.01$) and does not have significant impact on the overall performance of the cathode materials. Laine et al.[11] also investigated effect of magnesium doping to NCM811 cathode material. Mg was added to the metal sulfate solution with concentration targets of 0, 0.5 and 1 wt-% in the solution. These resulted 0,0.6 and 1.2 mol-% in the lithiated samples. Mg-doping lowered the specific capacity in early stages of cycling, but after prolonged (+800 cycles) cycling Mg-doped samples performed better than pure NCM. Mg-doping was also performing better while higher C-rates were applied in the cycling. Co-precipitated magnesium was observed evenly distributed in the samples.[11]

Use of calcium in a $Li_{1-2x}Ca_xCoO_2$ cathode materials has also been reported in literature. According to the studies of W.S. Yang et al.[12] and Z. Yang et al.,[13] the addition of electrochemically inactive calcium improves capacity retention of the material by occupying lithium sites in a layered structure and preventing phase transformation during lithium intercalation. Zinc is very rarely used as dopant, but it has also been added to cathode materials to prevent reactions between electrolyte and cathode material. Commonly ZnO-layer is coated on cathode materials, but also use of $ZnMn_2O_4$[14] and $Zn_3(PO_4)_2$[15] has been reported in literature. Potassium can be used as a precipitation chemical for precipitating metal hydroxides.[16] However, lower solubility of potassium sulfate does not encourage using KOH over NaOH for precipitating cathode material precursors.[17] Small amounts of K_2SO_4 originating from starting materials of co-precipitation probably does not have significant effect on overall alkali metal sulfate solubility.

In our previous study, we introduced method to selectively separate manganese from sparingly soluble sulfates present in zinc industry's manganese-rich anode sludge.[18] In solvent extraction purification over 99% zinc and iron content of the solution could be removed.[19] Aim of this research is to study applicability of manganese sulfate solutions containing impurities present in manganese sulfate solution obtained from industrial manganese sludge for synthesis of $LiNi_{0.8}Co_{0.1}Mn_{0.1}O_2$ cathode material.

Results and Discussion

Role of impurities in the co-precipitation of NMC811

NMC811 was co-precipitated and lithiated as described in Experimental section. First, the role of impurities (Mg, Ca, and Zn) was evaluated. Solubilities of magnesium, calcium and zinc were calculated using MEDUSA and HYDRA.[20,21] The concentrations that were used in the calculations were calculated based on the impurity concentrations present in the bulk of the reactor. Figure 1 shows solubilities of calcium (9 mg/L) and magnesium (1.1 mg/L left and 13.3 mg/L right) as a function of pH. Calcium concentration of the bulk solution starts to decrease at higher pH levels than operating conditions in bulk of the solution. However, mixing of the bulk solution with sodium hydroxide feed could have higher local pH than bulk of the reactor, which could precipitate $Ca(OH)_2$. Magnesium concentration starts to decrease around pH 10 depending on the starting concentration of the solution. Target pH 12.6 is marked with a vertical line to solubility curve of magnesium. Due to the high target pH, all present impurities except potassium were co-precipitated, which is also well in line with the earlier observations of Tan et al.[22] when hydroxide precipitation was used.

Figure 2 shows calculated solubilities of nickel, cobalt, manganese, iron and zinc in presence of 0.5 M ammonium ions. According to these calculations solubility minimum of iron and zinc is located to very close to targeted precipitation pH. Solubility minimums of Ni^{2+}, Co^{2+} and Mn^{2+} are also close to target pH of the precipitation.

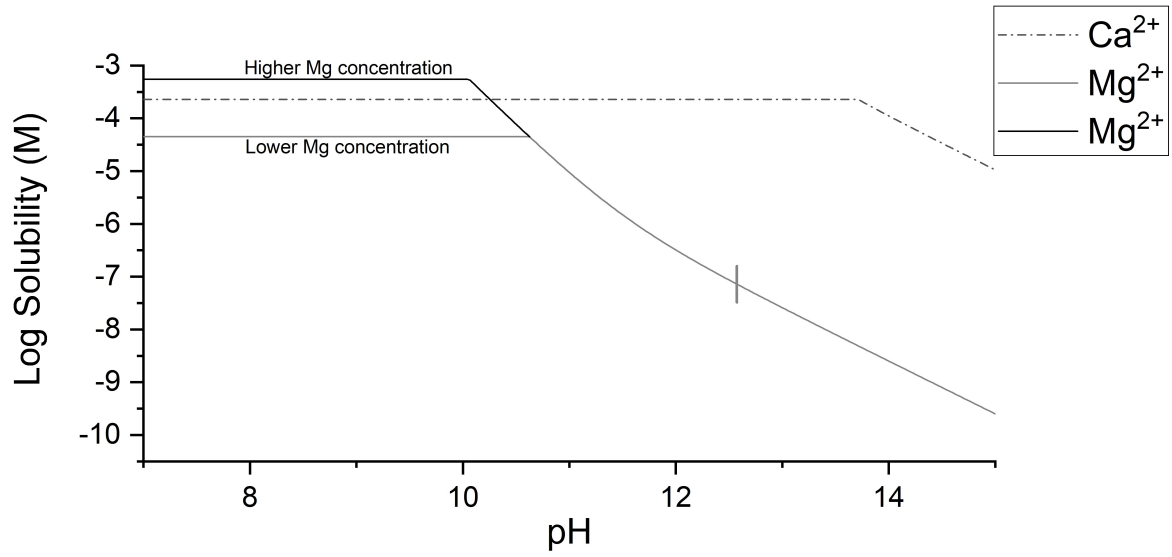

Figure 1. Calcium and magnesium solubilities as a function of pH. Calculated using MEDUSA and HYDRA.[20,21]

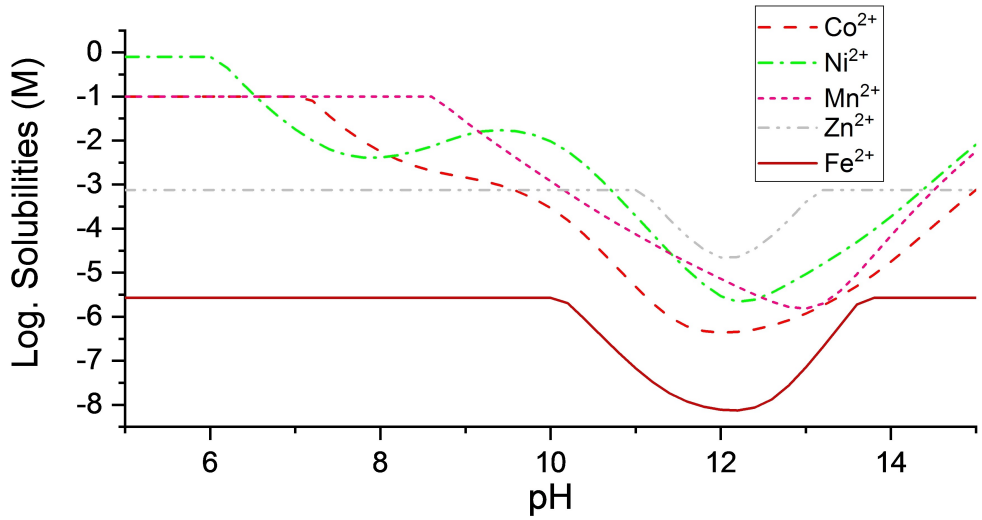

Figure 2. Solubilities of nickel, cobalt, manganese and zinc as a function of pH. Calculated using MEDUSA and HYDRA.[20,21]

Impurity contents in the prepared NMC811 precursors were measured by ICP-OES and ICP-MS. Table 1 shows impurity content of the precursors and calcinated $LiNi_{0.8}Co_{0.1}Mn_{0.1}O_2$. As can be seen in Table 1, calcium, zinc, magnesium and iron were co-precipitated as impurities to a large extent to these precursors. Potassium was not, as expected based on thermodynamic calculations.

Table 2 shows impurity concentrations of the filtrates at the end of the precipitation reactions. Calcium, magnesium, iron, and zinc contents of the bulk solution were almost completely co-precipitated during the precursor precipitation. Potassium is still present in the filtrate of the precipitation reaction. It was not detected in characterization of solid precipitates.

Table 3 shows molar ratios of prepared NCM cathode materials. Molar ratios of Ni and Co are very close to desired levels, but Mn appears to deviate from 10 mol-%. Particles were coated with aluminum to result 0.4 mol-% Al content on the prepared NCM 811 samples. Electrochemically inactive compounds, Ca, Fe, Mg and Zn, are only present at very low levels. Total impurity content of NCM811-Lo, NCM811-Mi and NCM811-Hi were only 0.025, 0.037 and 0.136 mol-%.

Figure 3 shows the XRD diffraction patterns of calcined samples. Table 4 summarizes crystallographic data for the prepared NCM811. All the main peaks in the XRD patterns and crystallographic data indicate that prepared cathode materials exhibit a hexagonal lattice structure with R3m space group (α-$NaFeO_2$ structure). No impurity phases were detected in XRD measurement. The clear splitting of the diffraction peaks (006)/(012) and (018)/(110) were observed from XRD patterns of all

Table 1. Impurity content of the prepared NMC811 precursors and lithiated samples, measured by ICP-OES and ICP-MS(*).

Precursors				
Sample	Ca	Mg*	Zn*	Fe*
	mg/kg	mg/kg	mg/kg	mg/kg
NCM811-Lo	31	<6	2.0	<10
NCM811-Mi	86	13	20.0	48
NCM811-Hi	80	127	449	42
Lithiated samples				
Sample	Ca	Mg*	Zn*	Fe*
	mg/kg	mg/kg	mg/kg	mg/kg
NCM811-Lo	62	22	13.5	24
NCM811-Mi	81	18	17	32
NCM811-Hi	104	122	428	29

Table 2. Impurity concentrations of the filtrates.

Sample	Ca	K	Mg	Zn	Fe
	mg/L	mg/L	mg/L	mg/L	mg/L
NCM811-Mi	1.7	260	0.21	0.5	<1
NCM811-Hi	<1	210	0.17	2	<1

Table 3. Molar ratios of prepared NCM 811 cathode materials.

Sample	Ni	Mn	Co	Al	Mg	Ca	Zn	Fe	Impurity (tot)
	[mol-%]	[mol-%]	[mol-%]	[mol-%]	[mol-%]	[mol-%]	[mol-%]	[mol-%]	[mol-%]
NCM811-Lo	80.8	9.3	9.5	0.40	0.009	0.015	0.002	0.004	0.025
NCM811-Mi	80.4	9.2	10.0	0.40	0.01	0.024	0.003	0.005	0.037
NCM811-Hi	80.4	9.1	10.1	0.41	0.052	0.025	0.063	0.005	0.136

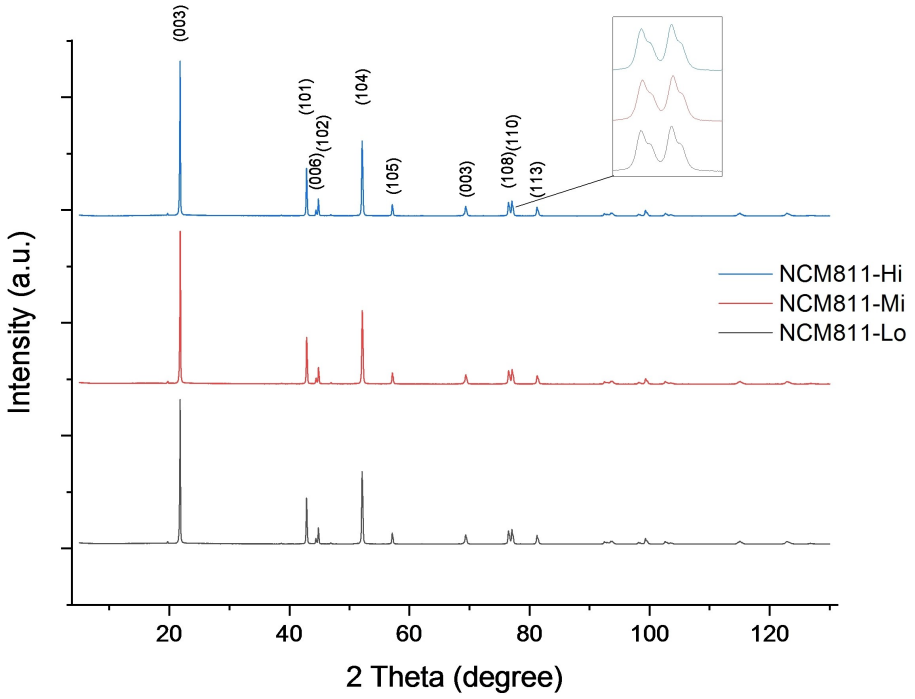

Figure 3. XRD patterns of prepared NCM811 cathode materials.

Table 4. Crystallographic data of the prepared NCM811.

Sample	a (Å)	c (Å)	c/3a	I(003)/(104)	(003) FWHM
NCM811-Lo	2.87197	14.2068	1.6489	1.269	0.123
NCM811-Mi	2.87188	14.2076	1.6491	1.307	0.123
NCM811-Hi	2.87172	14.2063	1.6490	1.283	0.118

samples. Rougier et al.[23] showed that lithium deficient $LiNiO_2$ does not exhibit splitting of diffraction peaks. Intensity ratios (003)/(104) indicate low cation mixing for all samples. Table 5 shows the lattice occupancies of the Li, Ni and O, which were determined by Rietveld refinement. Rietveld refinement confirmed that NCM811-Mi sample exhibited lowest cation mixing. It can be noted that well-crystalline LMO_2 phase was formed in every experiment of our work.

Scanning electron microscopy (FESEM) images of the co-precipitated precursors and NCM powders are shown in Figure 4. The micrometer-sized particles are of spherical shape,

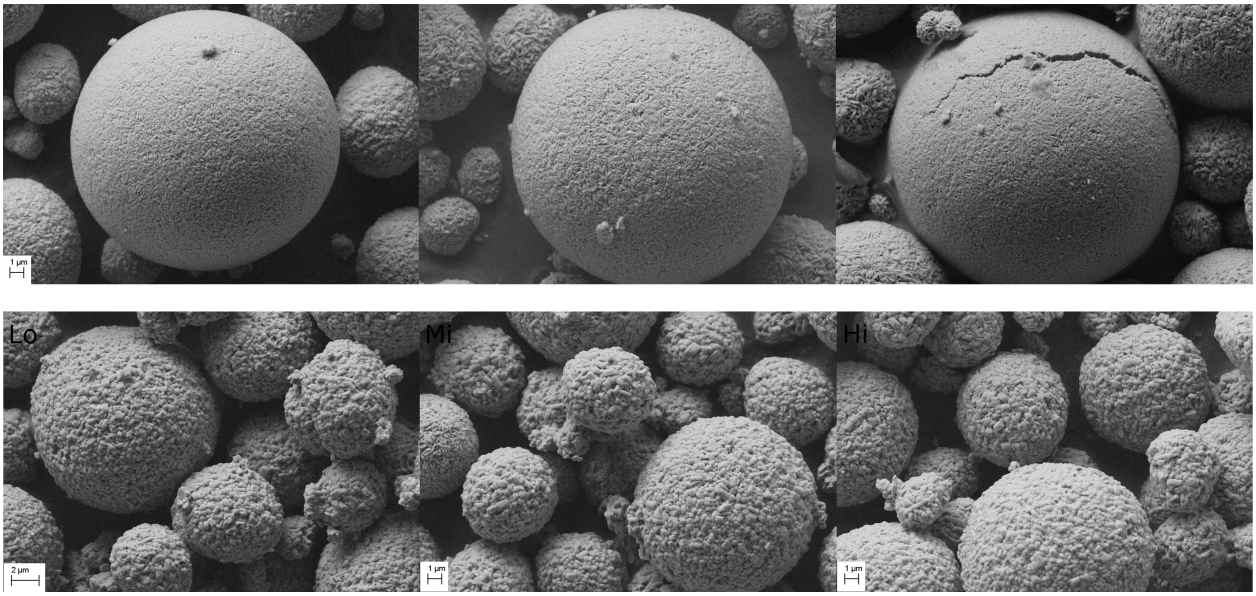

Figure 4. SEM images of metal hydroxide precursors (top) and lithium metal oxides after lithiation (below) with low, middle and high levels of impurities.

Table 5. Lattice occupancies of the Li, Ni, and O sites.

		NCM811-Lo	NCM811-Lo (EDS)	NCM811-Mi	NCM811-Mi (EDS)	NCM811-Hi	NCM811-Hi (EDS)
Li1	x	0	0	0	0	0	0
	y	0	0	0	0	0	0
	z	0.5	0	0.5	0	0.5	0
	Occ.	0.97488	0.00043	0.97714	0.00049	0.97708	0.00044
	B	0.5	0	0.5	0	0.5	0
Li2	x	0	0	0	0	0	0
	y	0	0	0	0	0	0
	z	0	0	0	0	0	0
	Occ.	0.02512	0.00043	0.02286	0.00049	0.02292	0.00044
	B	0.5	0	0.5	0	0.5	0
Ni1	x	0	0	0	0	0	0
	y	0	0	0	0	0	0
	z	0.5	0	0.5	0	0.5	0
	Occ.	0.02512	0.00043	0.02286	0.00049	0.02292	0.00044
	B	0.5	0	0.5	0	0.5	0
Ni2	x	0	0	0	0	0	0
	y	0	0	0	0	0	0
	z	0	0	0	0	0	0
	Occ.	0.97488	0.00043	0.97714	0.00049	0.97708	0.00044
	B	0.5	0	0.5	0	0.5	0
O1	x	0	0	0	0	0	0
	y	0	0	0	0	0	0
	z	0.25725	0.00005	0.25784	0.00006	0.25746	0.00005
	Occ.	1	0	1	0	1	0
	B	0.5	0	0.5	0	0.5	0
Rwp [%]		2.66%		3.07%		2.79%	

and they have the typical structure of secondary particles. It can be clearly seen from the higher magnification images that these secondary particles are made of densely packed primary particles. It can be noted from the SEM images of sample NCM811-Hi, that precursor particles had visible cracks in their structure. These defects were repaired during the calcination process. Figure 5 shows particle size distributions for precursors (A) and for lithiated cathode materials (B). Tap densities for samples were NCM811-Lo, NCM811-Mi and NCM811-Hi were 2.28, 2.14 and 2.16 g mL^{-1}.

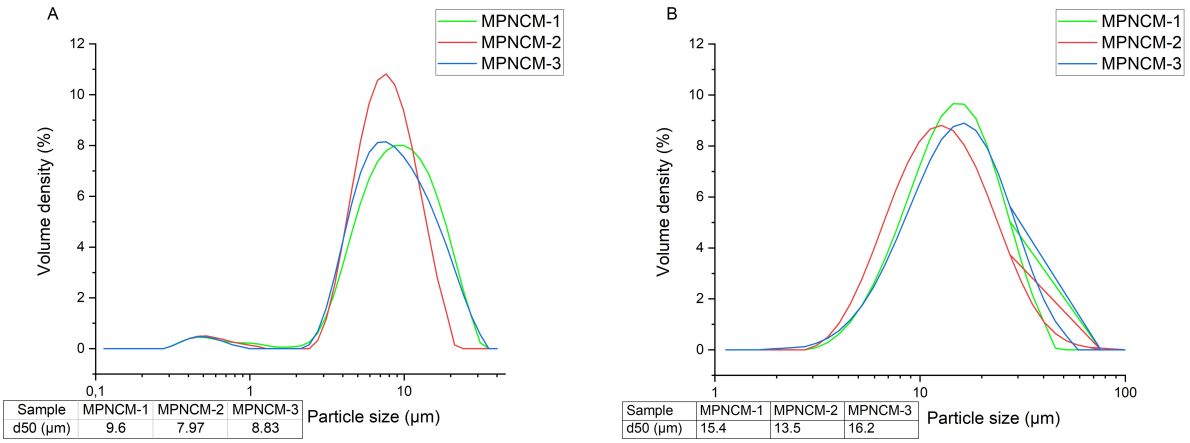

Figure 5. Particle size distributions of A) precursors and B) lithiated NCM cathode materials.

Effect of impurities on the cycling performance

In order to study effect of impurities on electrochemical performance of prepared LNCM samples, we carried out cycling tests between 2.6–4.3 V in coin cell and 2.8–4.2 V in pouch cell. Electrochemical performance for pouch cells was carried out with stress cycles using 1 C-rate followed by capacity checks after every 100 cycles using C-rate 0.2. Table 6 shows initial charge capacities, discharge capacities, first cycle efficiency, last cycle discharge capacity and capacity retention after 61 cycles. Initial discharge capacities of samples NCM811-Lo, NCM811-Mi and NCM811-Hi in coin cell were 202.9, 201 and 201.8 $mAhg^{-1}$. After 61 cycles capacity retention for all samples exceeded 92%. Figure 6 shows pouch cell discharge capacity retention at 0.2 C.and in pouch cell. Initial discharge capacities of samples NCM811-Lo, NCM811-Mi and NCM811-Hi in pouch cell were 185.1, 184.2 and 183 $mAhg^{-1}$. After 1100 cycles 81.1%, 80.6% and 80.6% capacity retention of the pouch cell samples were observed.

Li et al.[24] observed 78% capacity retention after 1000 cycles at 1 C rate for $LiNi_{0.8}Co_{0.1}Mn_{0.1}O_2$ cathode material using 4.2 V cut-off voltage. This is well in line with our results, however, Li et al.[24] did not use aluminium coating on their cathode material and there were small differences in the electrochemical cycling test.

During the first charge/discharge cycle pouch cells were charged at 0.03 C-rate and discharged at 0.1 C-rate. Figures 7a (coin half cells) and 7b (pouch cells) shows the initial charge-discharge curves for prepared cathode materials. First cycle is very identical for all samples. Miniscule negative effect of impurities can be noted during the first cycle.

Rate performances of prepared cathode materials are shown in Figure 8a. Both first and last cycles are very identical for all cathode material samples. Figure shows first and last discharge capacity of all samples. Figure 8b-d shows performance of cathode materials at various C-rates.

Summary and discussion

Two samples (NCM811-Mi and NCM811-Hi) were prepared from recycled manganese sulfate solution. These samples were compared to sample (NCM811-Lo) prepared from commercial manganese sulfate. Calcium, iron, magnesium and zinc were completely precipitated during the precursor co-precipitation. According to thermodynamic calculations zinc, iron and magnesium are precipitated in conditions prevalent bulk of the reactor, but calcium concentration should be lowered only at higher pH level. Proper conditions for calcium hydroxide precipitation could occur near the NaOH feeding tube, where bulk solution mixes with strong NaOH solution. Only impurity, which was still present in the filtrate was potassium, which was not detected in precursors or lithiated cathode materials. Total impurity content of the samples ranged from 0.025 to 0.136 mol-%. Measured nickel content of the reference sample was slightly higher than measured in two impure samples. Different manganese sulfate starting material could have had an impact on transition metal ratio. Tap density of the reference

Table 6. First cycle performance and capacity retention after 61 cycles.

Sample	1 st C 4.3 V 0.1 C + 0.015 C [mAh/g]	1st DC 2.6 V 0.1 C [mAh/g]	0.1 C Eff. [%]	2nd DC 2.6 V 0.1 C [mAh/g]	3rd DC 0.2 C [mAh/g]	61st DC 0.2 C [mAh/g]	Capacity retention [%]
NCM811-Lo	229.5	202.9	88.4	202.2	194.6	179.4	92.2
NCM811-Mi	223.3	201.0	90.0	200.7	193.4	179.6	92.9
NCM811-Hi	224.2	201.8	90.0	201.6	193.7	178.5	92.1

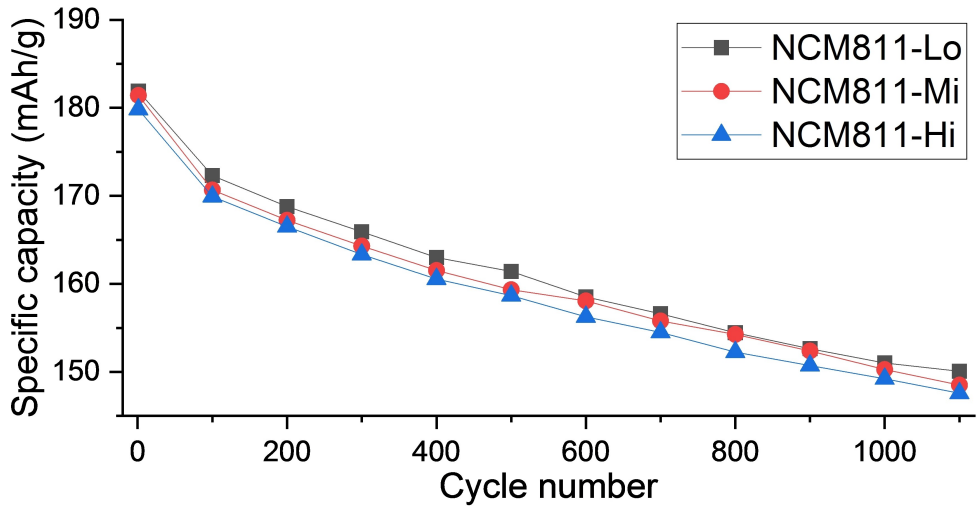

Figure 6. 0.2 C capacity checks between 1 C stress tests.

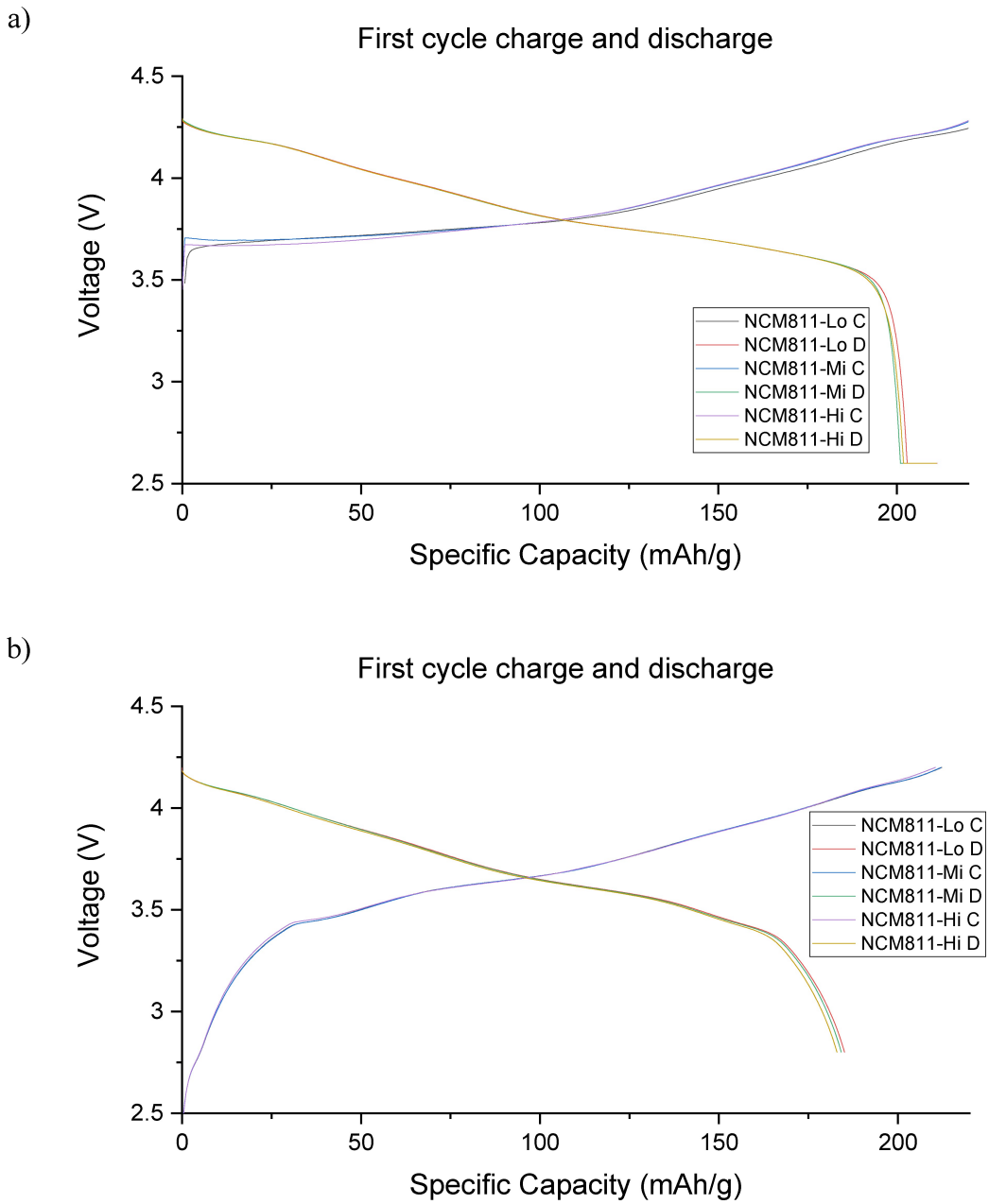

Figure 7. First cycle charge and discharge curves for a) coin half-cell samples and b) pouch cell samples.

sample was also slightly higher than for impure samples. Impurity content or slight alterations in main transition metal ratios did not show differences in crystallographic properties of prepared cathode materials. Co-precipitation followed by calcination produced spherical LNMC particles with identical particle size distribution. In electrochemical testing initial discharge capacities of impure samples were 0.5% and 1.1% lower than reference sample. Due to low content of impurities, variance in nickel content of the prepared samples could play more significant role determining rate performance of samples.

Conclusions

NCM811 cathode materials were successfully prepared by co-precipitation and calcination from three different metal sulfate solutions containing varying amounts of impurities. Elemental analysis showed precipitation of calcium, magnesium, zinc and iron. Potassium on the other hand did not precipitate during the hydroxide co-precipitation and is therefore found as a minor component in sodium sulfate containing filtrate. Despite various amounts of impurities present in the solid structure, all prepared samples exhibited well-crystalline LMO_2 structure and had spherical, dense morphology. Effects of impurities were minor to the cell performance. Half-cell electrochemical meas-

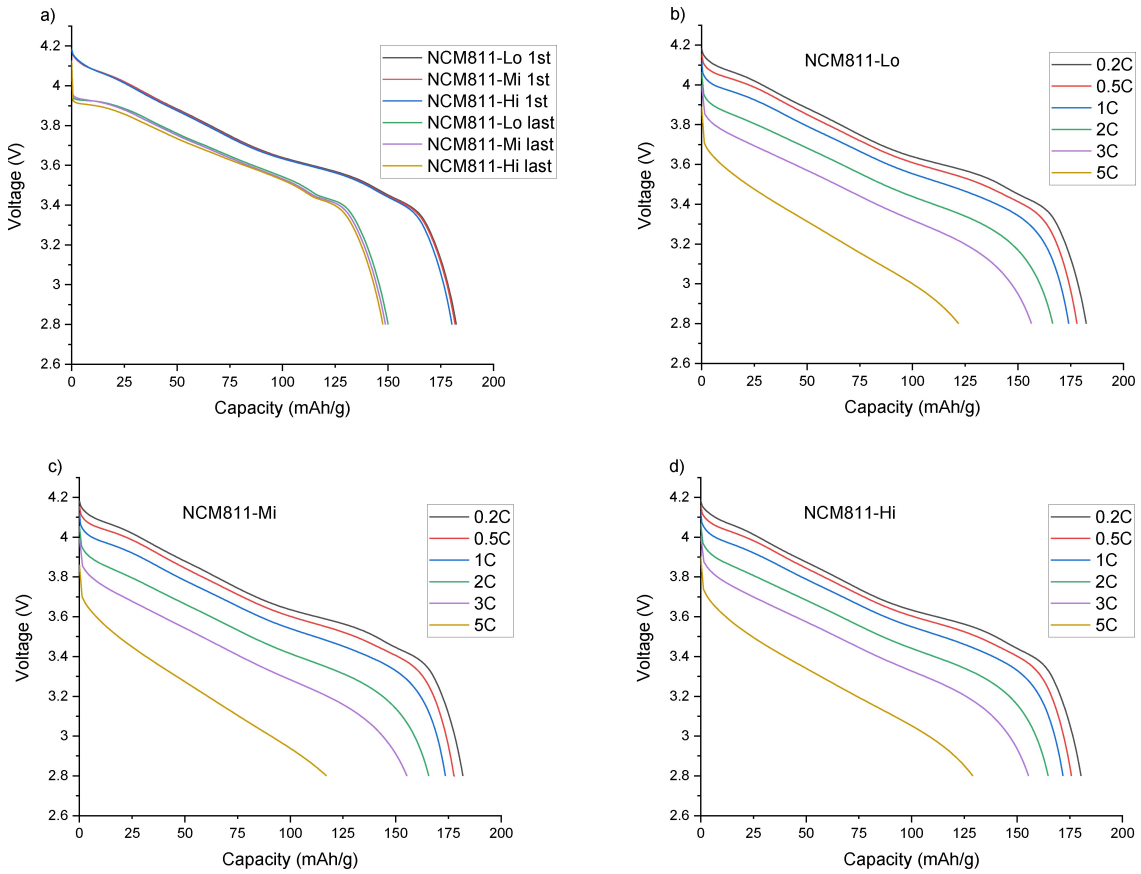

Figure 8. Electrochemical characterization of NCM811 samples in pouch cells at 25 °C. a) First cycle vs last cycle at C/5 rate, b–d) Discharge voltage profiles at various C-rates.

urements showed initial discharge capacity of >200 mAhg/g and capacity retention >92% after 61 cycles for all samples. Initial discharge capacity of all samples in pouch cell exceeded 183 mAhg/g. Capacity retention of all pouch cell samples were over 80% after 1100 cycles. The use of secondary raw materials in lithium-ion battery manufacturing is expected to increase. In this work secondary manganese obtained from low carbon roasting-leaching-electrowinning zinc manufacturing process, further purified, used in NCM811, and tested successfully.

Experimental Section

Raw materials and solutions for co-precipitation

In this research, the applicability of recycled manganese solutions for co-precipitation of NCM811 was studied. Three different sources of manganese sulfate were used in NCM811 precursor co-precipitation. Commercial manganese sulfate monohydrate powder (reference sample) and two different manganese sulfate solutions with different impurity content. Manganese sulfate solutions were prepared according to our previous work.[18] Manganese sulfate powder was dissolved in water to obtain corresponding solution to manganese sulfate solutions produced from anode sludge. Composition of the solid and liquid samples were determined using ICP-OES (Agilent 5110 VDV ICP-OES) and ICP-MS (Agilent 8900). ICP-OES analysis was performed to solid precipitates, and corresponding Li:Ni:Co:Mn ratio was confirmed. Microwave digestion was used for total dissolution of these samples without any leaching residue. This is done based on EPA3051A standard using nitric acid: hydrochloric acid with the ratio of 3:1 as solvent. Table 7 shows the composition of manganese sulfate solutions used in this study. Solution #1 is a commercial product. Manganese solution #2 is partly purified solution produced from manganese sludge. Solution #3 is produced from manganese sludge without purification.

Co-precipitation and lithiation of NCM811

Commercial bulk nickel sulfate and cobalt sulfate crystals were used in all experiments. 2M $MeSO_4$ solution was prepared by dissolving solids or mixing manganese sulfate solution to metal sulfate solution before diluting solution to the desired volume. Composition of used $MeSO_4$ solutions is presented in Table 8. Mn source #1 was used for NCM811-Lo, Mn source #2 was used for

Table 7. Composition of manganese sulfate solutions used in co-precipitation of NCM811 precursor. (ICP-OES).

Sample	Mn [g/l]	Zn [mg/L]	Ca [mg/L]	K [g/L]	Mg [mg/L]	Fe [mg/L]
1 (Reference)	180	<1	<1	<1	<1	<1
2	180	42	235	4.2	40	12.1
3	200	1800	220	3.9	490	26.1

Table 8. Composition of metal sulfate solutions used in co-precipitation.

Sample	Ni [g/L]	Co [g/L]	Mn [g/L]	Zn [mg/L]	Ca [mg/L]	K [mg/L]	Mg [mg/L]	Fe [mg/L]
NCM811-Lo	100.7	12.2	11.5	<1	3.5	<5	1.1	1.4
NCM811-Mi	95.4	11.7	10.8	3	19.1	253	2.3	1.7
NCM811-Hi	96.1	11.8	10.5	100	16.3	222	27	3.2

NCM811-Mi and Mn source #3 was used for NCM811-Hi. Sample names refer to the number of impurities in metal sulfate solutions, precursors and lithiated cathode materials.

Continuous stirred-tank reactor setup was used in co-precipitation experiments. Precursor hydroxides were co-precipitated by pumping 2 M $MeSO_4$, 5 M NaOH and 25 wt-% NH_4OH solutions into the reactor. pH of the reactor was kept constant at 12.6 by adjusting feeding rate of NaOH. Overhead stirrer at 1100 rpm mixed the reactor content. After feeding time of 33 to 34 hours, reaction was stopped, and solid precursor particles were separated by vacuum filtration. Obtained powder was then washed with excess of ion exchanged water. Washed NCM811 precursors were dried overnight in vacuum oven at 60 °C.

Dried hydroxide precursor (sieved <25 μm) was mixed with LiOH and $Al(OH)_3$ in molar ratio of $Li:(Ni_{0.8}Co_{0.1}Mn_{0.1}:Al)$ 1.04:(0.996:0.004). LiOH excess was used to compensate lithium loss during high temperature calcination and ensure homogenous lithiation. Al coating was used to prevent unwanted side reactions between electrolyte and active material.[25] The mixture calcined with 2.5 °C/min heating ramp and 6 h hold at 800 °C under O_2 flow. Material was milled and sieved <40 μm in dry room conditions. Residual lithium washed from surface with certain amount of deionized water and dried in vacuum oven.

Characterization of precursors and cathode powders

The microstructure shown by field emission scanning electron microscope (FESEM) images was obtained using a Zeiss Sigma FESEM operating at 5 kV at the Centre for Material Analysis of the University of Oulu.

X-ray diffraction (XRD) analysis was done for the calcined NCM811 cathode materials by using Rigaku SmartLab 9 kW with Co–Kα radiation at 40 kV and 135 mA. Diffractograms were collected in the 2θ range (5–120° at 0.01° intervals) with a scan speed of 4.06 deg/min. Diffraction peaks and crystallite parameters were identified using International Centre for Diffraction Data (PDF-4 + 2020). The crystallite sizes as well as anisotropy and distribution were computed using Rikagu PDXL2 analysis package. The Whole Powder Pattern Fitting (WPPF) was used with decomposition and least square Pawley method. The peak shape was modelled using FP (Fundamental Parameter) method with continuous scan and Cheary-Coelho Axial model using experimental geometry and optics. The crystallite shape is refined as ellipsoidal shape with lognormal distribution used as free parameters for iterative refinement other than spherical shape, which is better fit for crystal structure of NMC811. The site occupancy was analyzed using Rietveld model by PDXL2. Both XRD and FESEM were performed at the Centre for Material Analysis of the University of Oulu.

The tapped density of powders was measured using an Erweka SVM222 tapped density device and following the ISO EN 787/11 standard. Residual lithium was measured with an automatic titrator. Particle size distribution (PSD) during precipitation was measured with a Malvern Mastersizer 3000 (Malvern Pananalytical).

Electrochemical measurements/characterization

Cathode material was first sieved. Cathode slurry was mixed with Thinky are 250 mixer. Slurry composition was 4% of PVDF (Kureha #1100), 4% carbon (Timcal C45) and 92% active material and NMP as solvent. Cathode slurry was spread on aluminium foil with 100 μm applicator, then dried on hot plate at 50 °C for few hours and finally at vacuum oven at 120 °C overnight. Cathode foil was calendared three times before cell assembly. The active material loading on the foil was about 12 mg/cm^2. Theoretical capacity used to calculate the C-rate was 200 mAhg/g.

Electrochemical performance was carried out using one coin cell and one electrode pair pouch cell (50 mAhg). Coin cells were prepared with metallic lithium (Alfa Aesar 99.9% 0.75 mm foil) as a counter electrode and an electrolyte of 1 M LIPF6 in EC:DMC:EMC (1:1:1). Pouch cells were prepared with a graphite anode (Hitachi), an electrolyte of 1.15 M LIPF6 in EC:DMC:EMC (2:4:4), and 1% vinylene carbonate. All foils and cells were prepared in dry room.

Table 9 shows the C-rates used for coin cells. After the formation cycles, the pouch cells were at first charged at a constant current 1 C until 4.2 V was reached, and after that with a constant voltage until the current decreased to 0.03 C and discharged to 2.8 V at 1 C. Every 100 cycles, a capacity check cycle at 0.2 C was run and before the capacity check, the cells were discharged at 0.2 C.

Acknowledgements

Authors acknowledge Business Finland for research funding 2021–2024 (University of Oulu, BATCircle2.0, No. 44612/31/2020).

Conflict of Interests

The authors declare no conflict of interest.

Table 9. Coin cell testing program.

Cycle number	1	2	3	4	5	6	7-30	31	32-59	61
Charge C-rate	0.1 + 0.015	0.1 + 0.015	0.1 + 0.02	0.1 + 0.02	0.1 + 0.02	0.1 + 0.02	0.2 + 0.02	0.2 + 0.02	0.2 + 0.02	0.2 + 0.02
Discharge C-rate	0.10.015	0.1 + 0.015	0.2	0.33	0.5	1	2	0.2	2	0.2
Voltage range	4.3 V–2.6 V	4.3 V–2.6 V	4.3 V–3.0 V	4.3 V–3.0 V	4.3 V–3.0 V	4.3 V–3.0 V	4.3 V–3.0 V	4.3 V–3.0 V	4.3 V–3.0 V	4.3 V–3.0 V

Data Availability Statement

The data that support the findings of this study are available from the corresponding author upon reasonable request.

Keywords: Anode sludge · Cathode material · Manganese · NCM811 · Residue

[1] M. Winter, B. Barnett, K. Xu, *Chem. Rev.* **2018**, *118*, 11433–11456.
[2] S. Park, D. Kim, H. Ku, M. Jo, S. Kim, J. Song, J. Yu, K. Kwon, *Electrochim. Acta* **2019**, *296*, 814–822.
[3] M. S. Whittingham, *Chem. Rev.* **2004**, *104*, 4271–4301.
[4] H. Arai, S. Okada, Y. Sakurai, J. Yamaki, *Solid State Ionics* **1997**, *95*, 275–282.
[5] J. Välikangas, P. Laine, M. Hietaniemi, T. Hu, P. Tynjälä, U. Lassi, *Appl. Sci.* **2020**, *10*, 8988.
[6] S. Ahmed, A. Pokle, S. Schweidler, A. Beyer, M. Biachini, F. Walther, A. Mazilkin, P. Hartmann, T. Brezesinski, J. Janek, K. Volz, *ACS Nano* **2019**, *13*, 10694–10704.
[7] Y. Weng, S. Xu, G. Huang, C. Jiang, *J. Hazard. Mater.* **2013**, *246–247*, 163–172.
[8] "Rongbay Products", can be found under http://www.ronbaymat.com/index.php/En/Product, **2021** (accessed on 31 March 2023).
[9] J. Zheng, W. Hay Kan, A. Manthiram, *ACS Appl. Mater. Interfaces* **2015**, *7*, 6926–6934.
[10] J. Li, L. Wang, Q. Zhang, X. J. He, *J. Power Sources* **2009**, *189*, 28–33.
[11] P. Laine, M. Hietaniemi, J. Välikangas, T. Kauppinen, P. Tynjälä, S. Wang, H. Singh, U. Lassi, *Dalton Trans.* **2023**, *52*, 1413–1424.
[12] W. S. Yang, X. M. Li, L. Yang, D. G. Evans, X. Duan, *J. Phys. Chem. Solids* **2006**, *67*, 1343–1346.
[13] Z. Yang, W. Yang, Z. Tang, *J. Power Sources* **2008**, *184*, 557–561.
[14] X. Li, Y. Xu, *J. Solid State Electrochem.* **2008**, *12*, 851–855.
[15] J. Eom, J. Cho, *J. Electrochem. Soc.* **2008**, *155*, A201–A205.
[16] A. Delahaye-Vidal, B. Beaudoin, N. Sac-Epée, K. Tekaia-Elhsissen, A. Audemer, M. Figlarz, *Solid State Ionics* **1996**, *84*, 239–248.
[17] *Physical Constants of Inorganic Compounds in CRC Handbook of Chemistry and Physics* (Ed. D. R. Lide), Internet Version 2005, CRC Press, Boca Raton, Florida, **2005**.
[18] T. Kauppinen, T. Vielma, J. Salminen, U. Lassi, *ChemEngineering* **2020**, **4**, 40.
[19] N. Jantunen, T. Kauppinen, S. Virolainen, J. Salminen, U. Lassi, T. Sainio, *Miner. Eng.* **2021**, *173*, 107200.
[20] I. Puigdomenech, HYDRA: Hydrochemical Equilibrium-Constant Database, Royal Institute of Technology, Stockholm (Sweden), **2009**.
[21] I. Puigdomenech, MEDUSA: Make Equilibrium Diagrams Using Sophisticated Algorithms, Royal Institute of Technology, Stockholm (Sweden), **2010**.
[22] J. Tan, Q. Wang, S. Chen, Z. Li, J. Sun, W. Liu, W. Yang, X. Xiang, X. Sun, X. Duan, *Energy Storage Mater.* **2021**, *41*, 380–394.
[23] A. Rougier, P. Gravereau, C. J. Delmas, *Electrochem. Soc. Interface* **1996**, *143*, 1168.
[24] W. Li, X. Liu, Q. Xie, Y. You, M. Chi, A. Manthiram, *Chem. Mater.* **2020**, *32*, 7796–7804.
[25] S. Oh, J. K. Lee, D. Byun, W. I. Cho, B. W. Cho, *J. Power Sources* **2004**, *132*, 249–255..

Manuscript received: June 8, 2023
Revised manuscript received: July 12, 2023
Version of record online: ■■, ■■

RESEARCH ARTICLE

NCM811 cathode materials were prepared by co-precipitation and lithiation from metal sulfate solutions containing varying amounts of impurities (Ca, Mg, Zn, and Fe). All samples exhibited well-crystalline LMO_2 structure and spherical, dense morphology. Effects of impurities were minor to the cell performance.

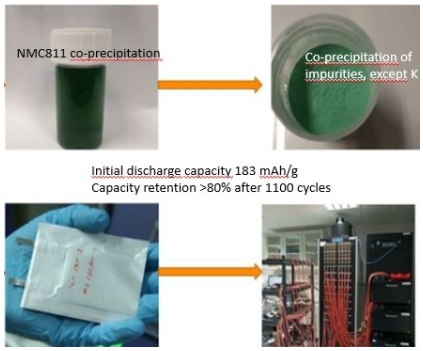

*T. Kauppinen, P. Laine, J. Välikangas, Dr. P. Tynjälä, Dr. T. Hu, Dr. J. Salminen, Prof. U. Lassi**

1 – 11

Co-precipitation of NCM 811 Using Recycled and Purified Manganese: Effect of Impurities on the Battery Cell Performance